CELADONITE AND SMECTITE FORMATION IN THE Úrkút Mn-CARBONATE ORE DEPOSIT (HUNGARY)

Márta Polgári[1], J.R. Hein[2], T. Németh[1], E. Pál-Molnár[3], T. Vigh[4]

[1]*Research Center for Astronomy and Geosciences, Institute for Geology and Geochemistry, Hungarian Academy of Sciences, Budapest, Hungary, 1112 Budapest, Budaörsi út. 45. e-mail: rodokrozit@gmail.com*

[2]*USGS, 400 Natural Bridges Dr., Santa Cruz*, CA 95060, U.S.A., *jhein@usgs.gov*

[3]*Szeged University, Dept. of Mineralogy, Geochemistry and Petrology, Egyetem str. 2-6, 6702 Szeged, Hungary, palm@geo.u-szeged.hu*

[4] *Mangán Ltd, Úrkút, Külterület 1. 8409 Hungary, manganvigh@vnet.hu*

ABSTRACT

Synsedimentary and early diagenetic oxygen levels are estimated by evaluating celadonite-smectite formation in marine Jurassic black shale-hosted manganese-carbonates. Celadonite formed under suboxic-dysaerobic conditions, Al-rich Fe-smectite formed at suboxic-anaerobic conditions, and nontronite formed at anoxic-anaerobic conditions during sedimentary burial. A genetic pathway by direct precipitation from solution is proposed for the enormous mass of celadonite, based on mineral and textural evidence. Lamination of the manganese ore is independent of clay-mineral composition and was given by a series of mineralized microbial Fe-rich biomats.

Key words: Jurassic, Mn carbonate ore, celadonite, nontronite, microbial Fe oxidation

1. Introduction

Clay minerals are useful environmental indicators. For example, the occurrence of kaolinite indicates intense acidic chemical leaching, whereas montmorillonite indicates a slightly alkaline

environment, reflecting the redox conditions at the modern ocean floor (Hein et al., 1979) and in pore waters during alteration of volcanic rocks (Bustillo and Martínez-Frías, 2003). However, for black shale-hosted Mn-carbonate ore assemblages, clay minerals have not been used even though the laminated nature and color of the deposits (brown-green-grey) indicate a possible clay-mineral utilization.

Investigations on the clay mineralogical composition of the Jurassic (Lias-Toarcian) Úrkút Mn deposit started in the early 1980s (Fig. 1), when smectite and authigenic celadonite, as main components of the fine grained rhodochrosite ore, were identified by XRD (Kaeding et al., 1983), suggesting clay minerals precipitated from porewater and/or seawater influenced by hydrothermal fluids. Varentsov et al. (1988) emphasized that these deposits resemble the nontronite-celadonite metalliferous sediments of marine hydrothermal areas (i.e. the Galapagos Rift Zone, southeast Pacific, Red Sea deeps), products of moderate to low-temperature hydrothermal systems formed in oxygen-deficient environments.

Alteration of volcanic material did not result in clay mineral formation in the Úrkút deposit (Polgári et al., 2012a) and Weiszburg et al. (2004) suggested that celadonite formed by authigenic precipitation from pore fluids. The minute size of the crystallites of the ore deposit made characterization of the clay minerals difficult. For celadonite, the dominant crystallite size is several tens of nm in thickness and some 100 to 1000 nm in length (Cora, 2008). The silicate flakes are chemically heterogenous and have various Fe-Al-Mg-Si ratios and K contents that are typical of interlayer-deficient micas (0.7-0.8 atoms per formula unit-a.p.f.u.; Weiszburg et al., 2004; Cora, 2008).

Smectite crystallites are several 100 nm long and very thin, with the dominant cations being K-Mg-Fe-Al. This silicate is also chemically heterogeneous and forms two subgroups, Al-rich Fe-

49 smectite and Al-poor Fe-smectite (Cora, 2008). The Mg and Fe contents are higher in the clay
50 minerals in laminae where Fe-rich minerals (pyrite, goethite) are abundant. The smectite is
51 mainly nontronite (Cora, 2008; Tóth et al., 2010).
52 The lamination of the ore is not mineralogically induced (Polgári et al., 2012b).
53 This paper determines the mineralogy, microstructure, and distribution of clay minerals
54 stratigraphically through the ore section; and the characterization of clay mineral genetic
55 pathways, which reflect fluctuations in redox conditions during ore formation.

56 **2. Geological setting and ore description**

57 The Jurassic (Lias, Toarcian) Úrkút Mn deposit is located in the Transdanubian Range (Fig. 1,
58 Fig. 2A). This black shale-hosted Mn-carbonate deposit is among the ten largest in the World. Its
59 reserves are 80 million tonnes of Mn-carbonate ore averaging 20 wt.% Mn and 10 wt.% Fe, with
60 an areal extent of tens of square kilometers. The ore deposit occurs within marine sedimentary
61 rocks composed mainly of bioclastic limestone, radiolarian clay marlstone, and dark-gray to
62 black shale. The Mn-carbonate ore beds comformably overlie middle Lias cherty limestone. The
63 rhodochrosite ore is composed of laminated, alternating gray, green, brown, and black sections
64 composed of mixtures of very fine-grained carbonate minerals and clay. Fine-grained (1–2 μm)
65 rhodochrosite rock lacks coarse and fine detrital clastics (Polgári et al., 2012a). Ore accumulation
66 took place in a structurally-controlled small marine basin in a low-energy, and low temperature
67 depositional environment. The deposit is unmetamorphosed, and was not effected by diagenetic
68 thermal overprint proved by stable O isotope data and interpretation (Polgári et al., 2012a). The
69 ore depost consists of three ore beds (10-, 3-, and 1 m thick), separated by a 20- and 4 m-thick
70 black shale (Fig. 2B).

A genetic model shows, that two cycles of bacterial activity triggered ore formation (Polgári et al., 2012a). Cycle 1 is a near-seabed aerobic chemolithoautotroph cycle which was essential in sequestering metal ions (Mn^{2+}, Fe^{2+}) from solution via enzymatic Mn(II) oxidation. Mn-oxide proto-ore was deposited in the sediment pile, serving as a paleoenvironmental indicator of oxic conditions. Cycle 2 represents an anaerobic/suboxic heterotrophic bacterial cycle in the frame of which early diagenetic bacterially mediated Mn(IV) and Mn(III) reduction processes took place via organic matter oxidation and Mn-carbonate mineralization (Polgári et al., 1991; Polgári et al., 2012a). The ore sequence is laminated in the millimeter scale (Fig. 2C, Fig. 3) reflecting a series of Fe-rich biomats (Polgári et al., 2012b). On a meter scale, the deposit shows color variations, the lower and upper part of the main ore bed is green and the middle part is brown. Towards the middle black shale, the top of the main ore bed is grey.

Fig. 1.

Fig. 2.

3. Samples and methods

X-ray powder diffraction on 56 samples (252 subsamples) was performed using a Philips diffractometer (PW 1710) with carbon monochromator and Cu Kα radiation, accelerating voltage - 45 kV and current - 35 mA Mineral composition was determined on randomly powdered samples by semi-quantitative phase analysis according to the modified direct method of Bárdossy et al. (1980), using previously defined intensity factors.

Oriented samples (112) were taken along a 917 cm complete section from the footwall to hanging wall from five sections dissecting the main ore bed and one section dissecting the upper ore beds (Fig. 2B). Bulk and separated lamina sub-samples were studied to determine

94 macroscopic features that cause color and grain-size variations. Ninety thin sections were studied
95 by microscopy.

96 **4. Results**

97 The Mn-carbonate ore beds are composed of Ca-rhodochrosite, celadonite, smectite, goethite,
98 and siderite. Moderate components are quartz, Mn-bearing calcite, apatite, pyrite, and barite; and
99 minor components are manganite, kutnohorite, gypsum, and feldspar (Fig. 4; Polgári et al.,
100 2012ab). Discrete nontronite layers of variable thicknesses occur in the ore deposit. Sub-lamina
101 XRD results show that celadonite and smectite occur separately in some laminae and in other
102 laminae both celadonite and nontronite occur, in variable amounts, and without recognizable
103 stratigraphic or spatial patterns.
104 Thin sections show that the entire ore bed is composed of a millimeter or thinner series of woven
105 structures, interpreted by Polgari et al. (2012b) as biomats (Fig. 3). The Fe-rich biomat structures
106 are composed of goethite. The matrix consists of Ca rhodochrosite, celadonite, and nontronite as
107 main components.
108 *Fig. 3.*
109 *Fig. 4.*

110 **5. Discussion**

111 **5.1. Authigenic mineral formation**

112 Recognition that Fe-rich biomats created the mm-scale lamination in the ore deposit makes it
113 possible to constrain the formation of authigenic clay minerals. The most probable microbial
114 Fe(II) oxidizing microbe was a *Gallionella*-like (*Mariprofundus ferrooxidans*) form living in a
115 neutrophylic, non-photosynthetic suboxic/dysaerobic environment (0.3 V Eh using recent
116 analogs; Konhauser, 1998; Hallbeck and Pedersen, 1990; Emerson et al., 2010). Most of the

117 modern seabed shows neutral pH conditions. Mineralogical and textural investigations show that
118 celadonite, goethite, and manganite formed at the sediment/water interface as synsedimentary
119 authigenic minerals.

120 **5.2. Celadonite formation**

121 The formation of celadonite has particular importance for understanding the genesis of the Úrkút
122 manganese ores. It is generally accepted that Fe-micas form preferentially (in limited quantities)
123 in submarine hydrothermal environments such as amygaloidal infilling and veinlets in basalt
124 (type 1, Pichler et al., 1991, Bustillo and Martínez-Frías, 2003), or during oxidic submarine
125 alteration of volcanic rocks (type 2, basaltic rocks, alteration rinds, often replaced or overgrown
126 by saponite; Butuzova et al., 1979, 1983; Varentsov et al., 1983). In addition, large
127 accumulations of hydrothermal green clays occur in mounds of the Galapagos Rift Zone, in
128 sediments of the East Pacific Rise and Bauer depression, in the spreading zones of the Gulf of
129 California, in the TAG and the Famous areas along the Mid-Atlantic Ridge, in Red Sea deeps,
130 and in the Gulf of Aden. Varentsov et al. (1988) interpreted the celadonitic phases in these green
131 clays as products of post-sedimentary (mainly diagenetic) transformation of Fe-smectite, which
132 in turn were formed in the initial crystallization stages of a siliceous-ferruginous gel under weak
133 reducing conditions (type 3; Butuzova et al., 1979, 1983; Varentsov et al., 1983).
134 These processes are highly unlikely at Úrkút because there are no volcanic rocks or substantial
135 amounts of volcanic debris. Nevertheless, there is an enormous amount of very fine-grained
136 celadonite, with an estimated mass of some tens to a hundred million tonnes based on ore reserve
137 and composition calculations. Detailed mineralogical observations (Weiszburg et al., 2004; Cora,
138 2008) indicate that celadonite directly precipitated from solution. Hence, celadonite is not a
139 diagenetic product from a precursor mineral phase (type 4, Úrkút; marine basin with distal

140 hydrothermal discharge and primary celadonite formation). Regardless of the differences in
141 precursor phases (rock, mineral, and solution), the formation of celadonite is similar. The
142 composition of celadonites from different formation types are similar, but textures (vein fillings,
143 alteration rinds), accompanying mineralogy (volcanic rock components), and chemical
144 composition distinguishes the four types of celadonite.
145 The Úrkút authigenic celadonite formed at low temperatures (17-23^{o} C; Polgári et al., 2012a).
146 Celadonite at Úrkút shows evidence for a slight variation in redox conditions (Fig. 5). It starts
147 from an oxidizing water-dominated environment (microbial Mn(II) enzymatic oxidation, aerobic
148 system with dissolved oxygen (DO) of more than 2 ml/l. That is followed by dysoxic conditions
149 (DO: 0.2-2.0 ml/l of H_2O) where microbial Fe(II) oxidation occurs (Fe-rich biomats, DO: 0.3
150 ml/l of H_2O), and then suboxic conditions (DO: 0-0.2 ml/l of H_2O), where primary celadonite
151 formation (DO: 0.1-0.2) occurs in a neutrophylic environment. DO values are based on Hallbeck
152 and Pedersen (1990), Wignall (1994), Konhauser (1998), Emerson et al. (2010), and the results
153 of nontronite synthesis laboratory experiments (Harder, 1976).
154 *Fig. 5.*
155 Conditions changed to a more reducing, sediment-dominated environment during burial, where
156 first Al-rich Fe-smectite and later Al-poor Fe-smectite (nontronite), formed. During this latter
157 stage, pyritization of goethite took place (Polgári et al., 2012b). Pyrite is always accompanied by
158 smectite, indicating reducing, anoxic conditions. Celadonite did not form from Fe-smectite
159 because the diagenetic process trends to oxygen depletion during increasing burial.
160 **5.3. Smectite formation**
161 The Úrkút smectites could have formed from (a) direct precipitation from hydrothermal fluids, as
162 like as nontronites in the modern ocean basins, characterized by Fe-rich compositions, low Al

and Mg, the presence of Ba, and relatively warm temperatures (T) (Bischoff, 1972; Cole and Shaw, 1983; Cole, 1983; Iizasa et al., 1998), or Red Sea brine smectites (Butuzova et al., 1979, 1983). However, relatively high temperatures (T) are not supported by O isotope results. A more probable mechanism is (b), low T reaction of Fe oxyhydroxide and silica, which is characterized by high Fe, low Al, and probably low Mg contents if formation took place with FeOOH formation; and moderate to high Fe, moderate Al, and low- to moderate Mg contents if the smectite formed at great distances from where FeOOH formed (Heath and Dymond, 1977; Polgári et al., 2012a).

According to Hein et al. (1979), two more general mechanisms can be presumed for the formation of authigenic smectite in the deep sea: (c) precipitation from solutions at low temperature into vesicles and fractures of basalts (seawater or leached from basalt by seawater), which are common at oceanic spreading centres (Seyfried et al., 1978); and (d) alteration of volcanic rock fragments and glass in the marine environment, which is the most commonly reported mechanism (Hein and Scholl, 1978; Bustillo and Martínez-Frías, 2003). Such smectites are characterized by a range of compositions, from Fe- and Mg-rich and moderate Al contents, to moderate to high Fe and Mg and higher Al contents than in types (a) and (b).

The composition of Úrkút smectites are Fe-Mg-rich with low Al and occasionally contain K (Polgári et al., 2012a), support formation by mechanisms (a) or (b). The (b) type smectite forms near the sediment-water interface where Mg is abundant and this may be the case for Úrkút, where the bottom waters were oxygenated (Polgári et al. 2012a), and consequently, smectite may not have formed until after some burial, perhaps 10-20 cm where conditions were more reducing (Hein et al., 1979). In this regard, smectite formed (Al-rich Fe-smectite) under more reduced

185 conditions than those under which celadonite formed, and nontronite formed in a fully reducing
186 environment, probably from celadonite or Al-rich Fe-smectite.
187 Another mechanism for nontronite and celadonite formation is through microbially mediated
188 processes (Köhler et al., 1994; Iizasa et al., 1998; Tazaki, 1997; Bustillo and Martínez-Frías,
189 2003). This mechanism cannot be excluded for the Úrkút, where a series of Fe-rich biomats
190 occur; however, microbially mediated diagenetic overprints probably eliminated primary textural
191 evidence for that process.

192 **5.4. Transformations of clay minerals and goethite**

193 On the basis of microscopy, the Fe-biomat texture is well preserved in most of the ore sections.
194 Only at the top part of the main and second goethite was transformed to pyrite. The textural
195 connection between well-preserved Fe-biomat goethite and the clay mineral matrix shows an
196 oxygen decrease from suboxic conditions, which probably occurred during early diagenesis after
197 some burial. Clay mineral-rich sediment accumulated prior to or at the same time as Fe-biomat
198 growth. The source of Fe(II) was most probably low T geothermal fluids ascending and mixing
199 with seawater (Polgári et al., 2012a). This is an aspect that needed clarification because the
200 microbially mediated goethite (originally ferrihydrite) reacting with silica can form clay minerals
201 as well, but textural observations do not support that sequence of events. Nontronite → goethite
202 and celadonite → goethite transformations are not considered likely because of Eh constraints;
203 the sediment pile did not become more oxic during diagenesis.

204 **6. Conclusion**

205 Clay minerals constrain the paleoenvironmental conditions during formation of the Úrkút Mn ore
206 deposit. The clay minerals formed synchronously in different parts of the sediment column under
207 different redox conditions, celadonite at the sediment/water interface or very close to it, and

smectite in the deeper, more reducing parts. A pathway of celadonite formation is proposed by direct precipitation from solution en masse. Nontronite formed in the reducing part of the sediment column. These results show that celadonite and nontronite indicate palaeo-oxygen level fluctuations in the environment. Biomats reflect suboxic conditions, which changed to anoxic with increasing burial. Color in the Úrkút deposit does not reflect oxygen conditions as commonly thought; for example, brown can be anoxic (nontronite) and green suboxic (celadonite), so color as a paleoproxy must be used with caution.

Acknowledgments

The study was supported by Hungarian Science Foundation (OTKA-NKTH No. K 68992).

References

Bárdossy, G., Bottyán, L., Gadó, P., Griger, Á., Sasvári, J., 1980. Automated quantitative phase analysis of bauxites. American Mineralogist **65,** 135–141.

Bischoff, J.L., 1972. A ferroan nontronite from the Red Sea geothermal system. Clays and Clay Minerals 20, 217-223.

Bustillo, M.A., and Martinez-Frias, J., 2003. Green opals in hydrothermalized basalts (Tenerife Island, Spain): alteration and aging of silica pseudoglass. Journal of Non-Cristalline Solids 323, 1-3, 27-33.

Butuzova, G.Y., Drits, V.A., Lisitsyna, N.A., Tsipurskiy, S.I., and Dmitrik, A.L., 1983. New data on authigenic layered silicates in the metalliferous sediments of the Atlantis II deep, Red Sea. Litologia i poleznye iskopaemye 5, 82-88.

229 Cole, T.G., 1983. Oxygen isotope geothermometry and origin of smectites in the Atlantis II
230 Deep, Red Sea. Earth Planet. Sci. Lett. 66, 166-176.
231 Cole, T.G., and Shaw, H.F., 1983, The nature and origin of authigenic smectites in some recent
232 marine sediments: Clay Miner., v. 18, p. 239-252.
233 Cora, I., 2008. Mineralogical study of the Úrkút Mn carbonate ore [Ms. Dissertation]. Budapest,
234 Eötvös Loránd University, 120 p.
235 Emerson, E., Fleming, E.J., and McBeth, J.M., 2010. Iron-oxidizing bacteria: an environmental
236 and genomic perspective. Ann. Rev. Microbiol. 64, 561-583.
237 Hallbeck, L. and Pedersen, K., 1990. Culture parameters regulating stalk formation and growth
238 rate of Gallionella ferruginea. J. Gen. Microbiol. 136, 1675-1680.
239 Harder, H., 1976. Nontronite synthesis at low temperatures. Chemical Geology 18, 169-180.
240 Harder, H., 1978. Synthesis of iron layer silicate minerals under natural conditions. Clays and
241 Clay Minerals 26, 65-72.
242 Heath, G.R., and Dymond, J., 1977. Genesis and transformation of metalliferous sediments from
243 the East Pacific Rise, Bauer Deep, and Central Basin, northwest Nazca plate. Geol. Soc. Am.
244 Bull. 88, 723-733.
245 Hein, J.R. and Scholl, D.W., 1978. Diagenesis and distribution of Late Cenozoic volcanic
246 sediment in the southern Bering Sea. Geological Society America Bulletin 89, 197-210.
247 Hein, J.R., Yeh, H-W., and Alexander, E., 1979. Origin of iron- rich montmorillonite from the
248 manganese nodule belt of the North equatorial Pacific. Clays and Clay Minerals 27, 185-194.
249 Iizasa, K., Kawasaki, K., Maedas, K., Matsumoto, T., Saito, N., and Hirai, K., 1998.
250 Hydrothermal sulfide-bearing Fe-Si oxyhydroxide deposits from the Coriolis Trough,
251 Vanuatu back arc, southwestern Pacific. Marine Geology 145, 1-21.

252 Kaeding, L., Brockamp, O., and Harder, H., 1983. Submarin-Hydrothermale Entstehung der
253 Sedimentaren Mn-Lagerstatte Úrkút (Ungarn). Chemical Geology 40, 251-268.
254 Köhler, B., Singer, A., and Stoffers, P., 1994. Biogenic nontronite from marine white smoker
255 chimneys. Clays and Clay Minerals 42, 6, 689-701.
256 Konhauser, K.O., 1998. Diversity of bacterial iron mineralization. Earth Science Reviews 43, 91-
257 121.
258 Pichler, T., Ridley, W.I., and Nelson, E., 1999. Low-temperature alteration of dredged volcanics
259 from the Southern Chile Ridge: additional information about early stage of seafloor
260 weathering. Marine Geology 159, 155-177.
261 Polgári, M, Hein, J.R., Tóth, A.L., Pál-Molnár, E., Vigh, T., Bíró, L., and Fintor, K., 2012b.
262 Microbial action formed Jurassic Mn-carbonate ore deposit in only a few hundred years
263 (Úrkút, Hungary). Geology 40, 10, 903-906.
264 Polgári, M., Hein, J.R., Vigh, T., Szabó-Drubina, M., Fórizs, I., Bíró, L., Müller, A., and Tóth,
265 A.L., 2012a. Microbial processes and the origin of the Úrkút manganese deposit, Hungary.
266 Ore Geology Reviews 47, 87-109, doi: 10.1016/j.oregeorev.2011.10.001.
267 Polgári, M., Okita, P.M., and Hein, J.R., 1991. Stable isotope evidence for the origin of the Úrkút
268 manganese ore deposit, Hungary. Journal of Sedimentary Petrology 61, 3, 384-393.
269 Seyfried, W.E.J., Shanks, W.C.I., and Dibble, W.E.J., 1978. Clay mineral formation in DSDP leg
270 34 basalt. Earth and Planet. Sci. Letters 41, 265-276.
271 Szabó, Z, Grasselly, Gy., 1980. Genesis of manganese oxide ores in the Úrkút Basin, Hungary:
272 *in*: Varentsov, I.M,, Grasselly, Gy, eds,. Geology and Geochemistry of Manganese, vol. 2.
273 Budapest Akadémiai Kiadó, 223– 36.

Tazaki, K., 1997. Biomineralization of layer silicates and hydrated Fe/Mn oxides in microbial mats: an electron microscopical study. Clays and Clay Minerals, 45, 203-212.

Tóth, E., Weiszburg, G.T., Jeffries, T., Williams, C.T., Bartha, A., Bertalan, É., Cora, I., 2010, Submicroscopic accessory minerals overprinting clay mineral REE patterns (celadonite-glauconite group examples): Chemical Geology, 269, 312-328.

Tyson R.V., Pearson T.H., 1991. Modern and ancient continental shelf anoxia: an overview: *in* Tyson, R.V., Pearson, T.H. eds., Modern and anciuent continental shelf anoxia, Geological Society Special Publication, 58, 1-26.

Varentsov, I.M., Grasselly, Gy., and Szabó, Z., 1988. Ore-formation in the early-Jurassic basin of Central Europe: Aspects of mineralogy, geochemistry and genesis of the Úrkút manganese deposit, Hungary. Chemie der Erde 48, 257-304.

Varentsov, I.M., Sakharov, B.A., Drits, V.A., Tsipursky, S.I., Choporov, D.Ya., and Aleksandrova, V.A., 1983. Hydrothermal deposits of the Galapagos Rift Zone, Leg 70: Mineralogy and geochemistry of major components: *in* Honnorez, J., von Herzen, R.P., et al., eds., Initial Reports of the Deep Sea Drilling Project, v. 70, U.S. Govt. Printing Office, Washington, p. 235-268.

Weiszburg, T. G., Tóth, E., and Beran, A., 2004. Celadonite, the 10-Å green clay mineral of the manganese carbonate ore, Úrkút, Hungary. Acta Miner. Petr. Szeged. 45, 65-80.

Wignall, P.B., 1994. Black shales: Oxford, UK, Clarendon Press, 124 p.

Figure captions

Fig. 1. Geological sketch map of the Úrkút manganese deposit (after Szabó and Grasselly, 1980). The locality GPS data: 47°04′55″N; 17°38′40″E

297 Fig. 2. Locality map (A), Geological profile with sample locations of the Úrkút Mn-carbonate
298 deposit (B). (Sampling 2009, Úrkút Mine, Shaft No. III, deep level, +180 m; total No. of
299 samples 112 spanning 917 cm from the base to the top of the three ore layers and the
300 intervening black shale). Key: fragm-fragmented sample; cont.-continuous sampling; not
301 cont.-not continuous sampling; numbers on the stratigraphic columns are sample
302 numbers; * indicates samples for XRD; 0 indicates samples for thin sections (in brackets
303 the number of thin sections, total 90); Profiles 1, 3, 4, 5 are from main ore bed, Profile Za
304 and Zb are from second ore bed. Patterns show only color varieties and not sedimentary
305 structures; (C1) green (C2) brown Mn-carbonate ore.
306 Fig. 3. Thin section photos showing Fe-rich biomat structures for different representative
307 samples and magnifications. The thickness of the thin sections and the density of biomats
308 are variable. Arrows show representative parts of mineralized filamentous structures. For
309 sample locations see Fig. 1.
310 Fig. 4. Mineral composition (XRD) of Mn-carbonate ore samples and macroscopically separated
311 subsamples normalized to 100% (for sample locations see Fig. 1). The graph was made
312 by coding the estimated quantity of selected minerals (graphics by Gergely Rózsás,
313 Pázmány Péter University). Key: gry-grey; grn-green; brn-brown; blk-black; avg-average.
314 Fig. 5. Estimated formation conditions of the clay minerals in the black shale-hosted Mn
315 carbonate ore deposit (Úrkút), zone of microbial Fe(II) oxidation (+0.3 V Eh using recent
316 analogs; Konhauser, 1998; Hallbeck and Pedersen, 1990; Emerson et al., 2010), and the
317 results of nontronite synthesis laboratory experiments (by dashed lines, Harder, 1976,
318 1978). Note: in general oxidizing conditions mean high oxygen concentration (high Eh

values up to +0.4V), while reduced conditions reveal a lack of oxygen (low Eh down to -0.2V. Eh estimation is based on Wignall, 1994).

321 Fig. 1.

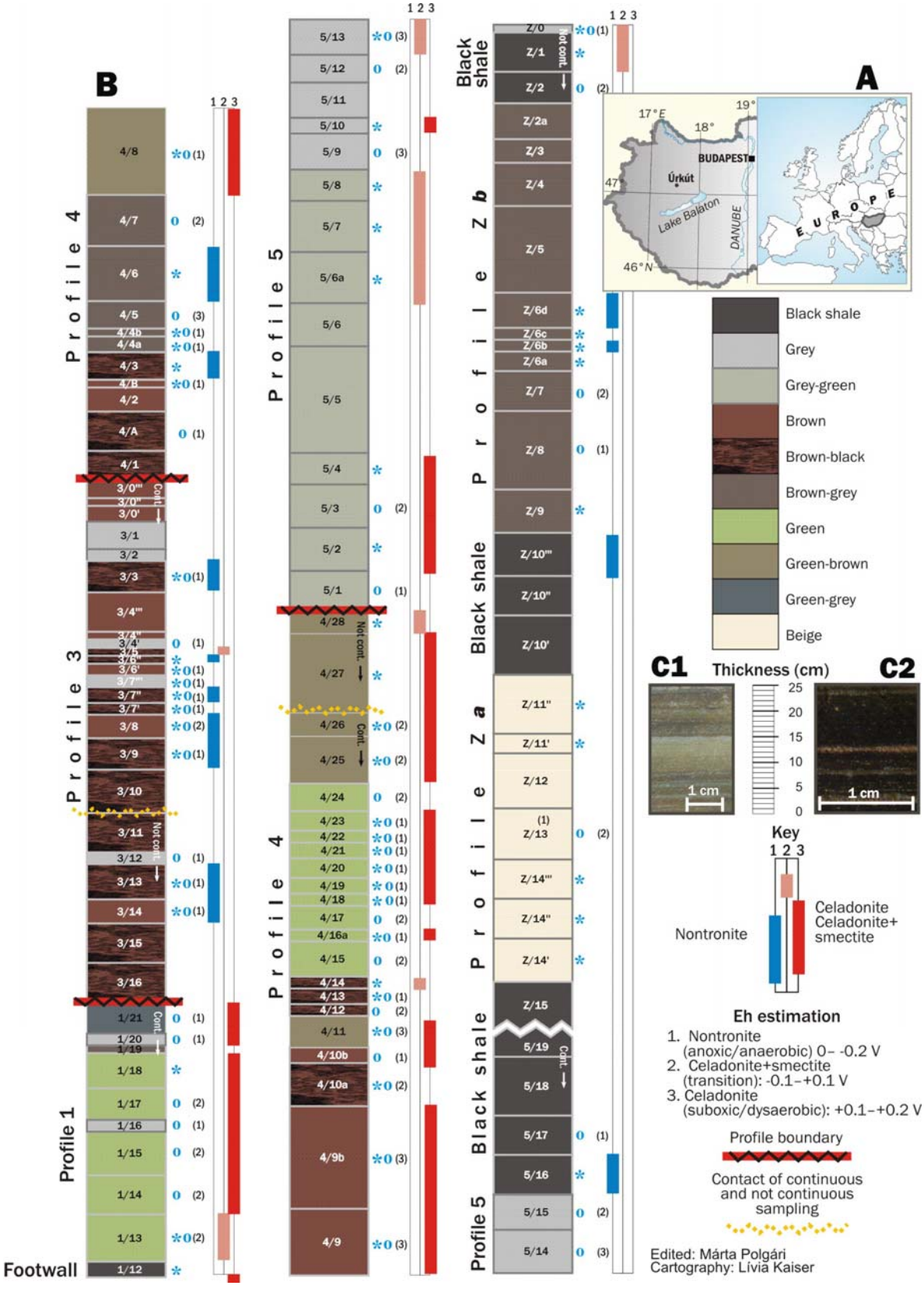
B
A
Profile 1
Profile 3
Profile 4
Profile 5
Black shale
Profile Zb
Profile Za
Footwall
Not cont.
Cont.
1 2 3
BUDAPEST
Úrkút
Lake Balaton
DANUBE
17°E
18°
19°
47°
46°N
EUROPE
Black shale
Grey
Grey-green
Brown
Brown-black
Brown-grey
Green
Green-brown
Green-grey
Beige
C1
C2
Thickness (cm)
1 cm
Key
Nontronite
Celadonite
Celadonite+ smectite
Eh estimation
1. Nontronite (anoxic/anaerobic) 0– -0.2 V
2. Celadonite+smectite (transition): -0.1–+0.1 V
3. Celadonite (suboxic/dysaerobic): +0.1–+0.2 V
Profile boundary
Contact of continuous and not continuous sampling
Edited: Márta Polgári
Cartography: Lívia Kaiser

Fig. 2.

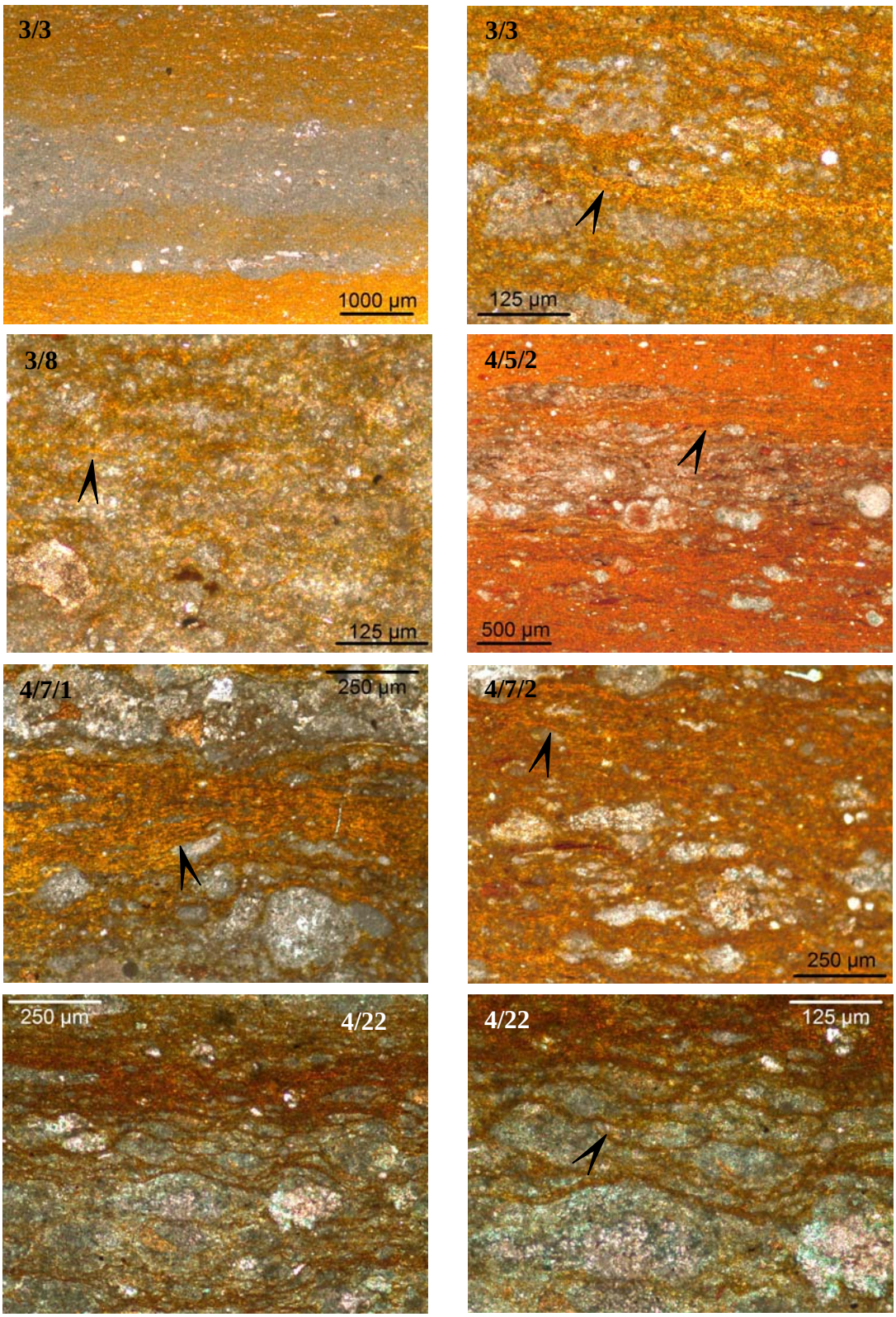
3/3
1000 µm
3/3
125 µm
3/8
125 µm
4/5/2
500 µm
4/7/1
250 µm
4/7/2
250 µm
250 µm
4/22
4/22
125 µm

Fig. 3.

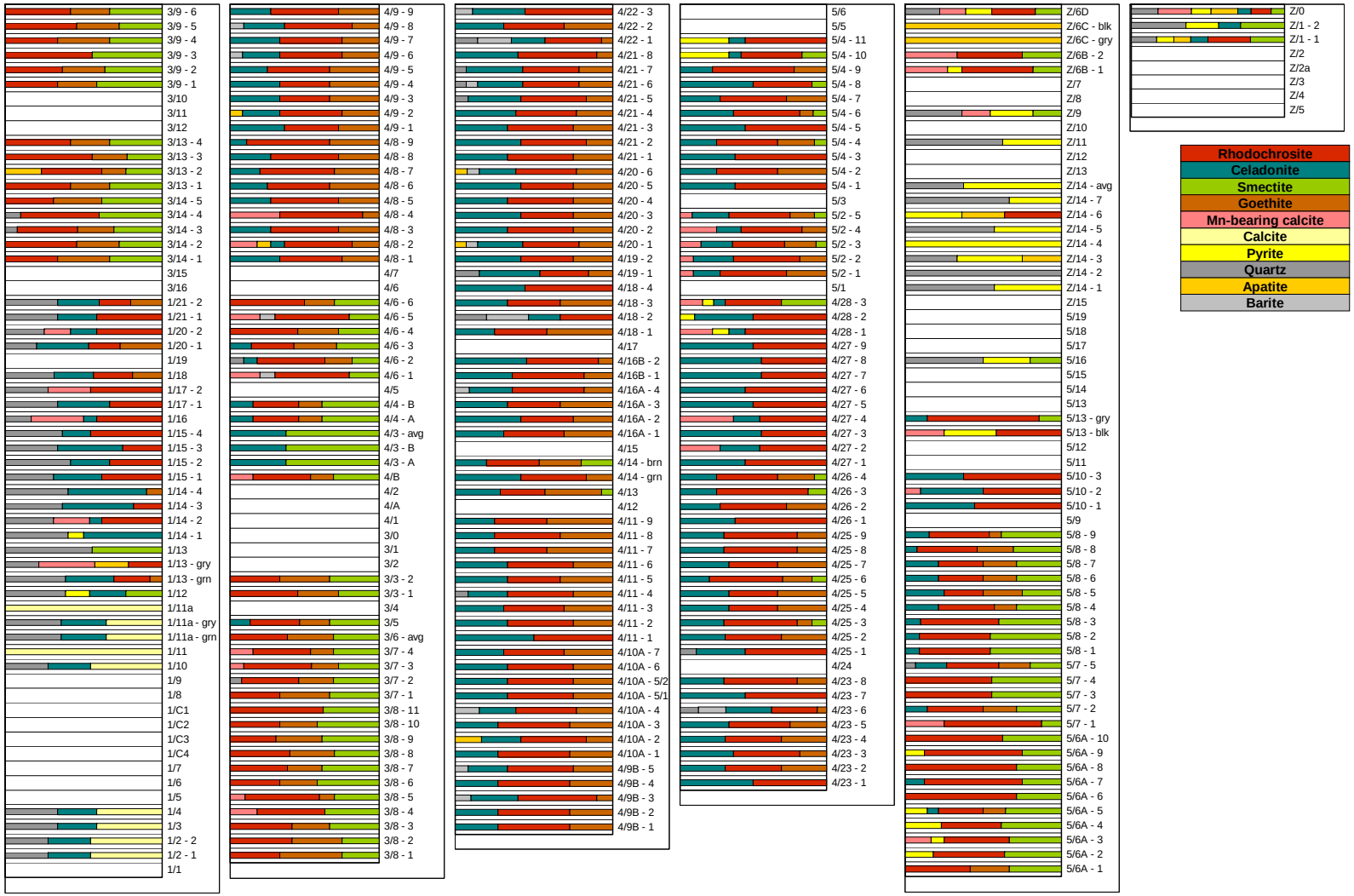
3/9 - 6
3/9 - 5
3/9 - 4
3/9 - 3
3/9 - 2
3/9 - 1
3/10
3/11
3/12
3/13 - 4
3/13 - 3
3/13 - 2
3/13 - 1
3/14 - 5
3/14 - 4
3/14 - 3
3/14 - 2
3/14 - 1
3/15
3/16
1/21 - 2
1/21 - 1
1/20 - 2
1/20 - 1
1/19
1/18
1/17 - 2
1/17 - 1
1/16
1/15 - 4
1/15 - 3
1/15 - 2
1/15 - 1
1/14 - 4
1/14 - 3
1/14 - 2
1/14 - 1
1/13
1/13 - gry
1/13 - grn
1/12
1/11a
1/11a - gry
1/11a - grn
1/11
1/10
1/9
1/8
1/C1
1/C2
1/C3
1/C4
1/7
1/6
1/5
1/4
1/3
1/2 - 2
1/2 - 1
1/1
4/9 - 9
4/9 - 8
4/9 - 7
4/9 - 6
4/9 - 5
4/9 - 4
4/9 - 3
4/9 - 2
4/9 - 1
4/8 - 9
4/8 - 8
4/8 - 7
4/8 - 6
4/8 - 5
4/8 - 4
4/8 - 3
4/8 - 2
4/8 - 1
4/7
4/6
4/6 - 6
4/6 - 5
4/6 - 4
4/6 - 3
4/6 - 2
4/6 - 1
4/5
4/4 - B
4/4 - A
4/3 - avg
4/3 - B
4/3 - A
4/B
4/2
4/A
4/1
3/0
3/1
3/2
3/3 - 2
3/3 - 1
3/4
3/5
3/6 - avg
3/7 - 4
3/7 - 3
3/7 - 2
3/7 - 1
3/8 - 11
3/8 - 10
3/8 - 9
3/8 - 8
3/8 - 7
3/8 - 6
3/8 - 5
3/8 - 4
3/8 - 3
3/8 - 2
3/8 - 1
4/22 - 3
4/22 - 2
4/22 - 1
4/21 - 8
4/21 - 7
4/21 - 6
4/21 - 5
4/21 - 4
4/21 - 3
4/21 - 2
4/21 - 1
4/20 - 6
4/20 - 5
4/20 - 4
4/20 - 3
4/20 - 2
4/20 - 1
4/19 - 2
4/19 - 1
4/18 - 4
4/18 - 3
4/18 - 2
4/18 - 1
4/17
4/16B - 2
4/16B - 1
4/16A - 4
4/16A - 3
4/16A - 2
4/16A - 1
4/15
4/14 - brn
4/14 - grn
4/13
4/12
4/11 - 9
4/11 - 8
4/11 - 7
4/11 - 6
4/11 - 5
4/11 - 4
4/11 - 3
4/11 - 2
4/11 - 1
4/10A - 7
4/10A - 6
4/10A - 5/2
4/10A - 5/1
4/10A - 4
4/10A - 3
4/10A - 2
4/10A - 1
4/9B - 5
4/9B - 4
4/9B - 3
4/9B - 2
4/9B - 1
5/6
5/5
5/4 - 11
5/4 - 10
5/4 - 9
5/4 - 8
5/4 - 7
5/4 - 6
5/4 - 5
5/4 - 4
5/4 - 3
5/4 - 2
5/4 - 1
5/3
5/2 - 5
5/2 - 4
5/2 - 3
5/2 - 2
5/2 - 1
5/1
4/28 - 3
4/28 - 2
4/28 - 1
4/27 - 9
4/27 - 8
4/27 - 7
4/27 - 6
4/27 - 5
4/27 - 4
4/27 - 3
4/27 - 2
4/27 - 1
4/26 - 4
4/26 - 3
4/26 - 2
4/26 - 1
4/25 - 9
4/25 - 8
4/25 - 7
4/25 - 6
4/25 - 5
4/25 - 4
4/25 - 3
4/25 - 2
4/25 - 1
4/24
4/23 - 8
4/23 - 7
4/23 - 6
4/23 - 5
4/23 - 4
4/23 - 3
4/23 - 2
4/23 - 1
Z/6D
Z/6C - blk
Z/6C - gry
Z/6B - 2
Z/6B - 1
Z/7
Z/8
Z/9
Z/10
Z/11
Z/12
Z/13
Z/14 - avg
Z/14 - 7
Z/14 - 6
Z/14 - 5
Z/14 - 4
Z/14 - 3
Z/14 - 2
Z/14 - 1
Z/15
5/19
5/18
5/17
5/16
5/15
5/14
5/13
5/13 - gry
5/13 - blk
5/12
5/11
5/10 - 3
5/10 - 2
5/10 - 1
5/9
5/8 - 9
5/8 - 8
5/8 - 7
5/8 - 6
5/8 - 5
5/8 - 4
5/8 - 3
5/8 - 2
5/8 - 1
5/7 - 5
5/7 - 4
5/7 - 3
5/7 - 2
5/7 - 1
5/6A - 10
5/6A - 9
5/6A - 8
5/6A - 7
5/6A - 6
5/6A - 5
5/6A - 4
5/6A - 3
5/6A - 2
5/6A - 1
Z/0
Z/1 - 2
Z/1 - 1
Z/2
Z/2a
Z/3
Z/4
Z/5
Rhodochrosite
Celadonite
Smectite
Goethite
Mn-bearing calcite
Calcite
Pyrite
Quartz
Apatite
Barite

Fig. 4.

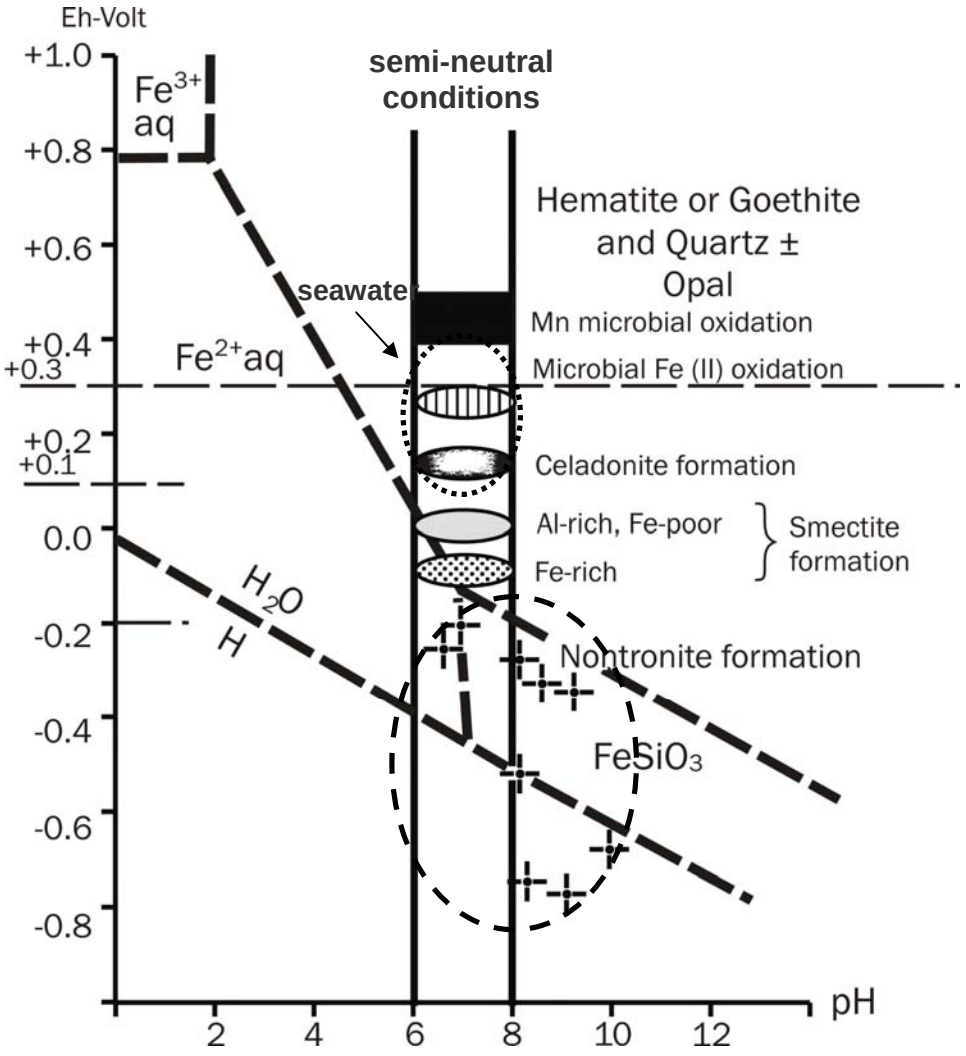
Eh-Volt
+1.0
+0.8
+0.6
+0.4
+0.3
+0.2
+0.1
0.0
-0.2
-0.4
-0.6
-0.8
Fe3+ aq
Fe2+aq
H2O
H
semi-neutral conditions
seawate
Hematite or Goethite and Quartz ± Opal
Mn microbial oxidation
Microbial Fe (II) oxidation
Celadonite formation
Al-rich, Fe-poor
Fe-rich
Smectite formation
Nontronite formation
FeSiO3
2
4
6
8
10
12
pH

446
447
448
449
450
451
452
453
454
455
456
457
458
459
460
461
462
463
464
465
466
467
468
469
470
471
472
473
474
475
476
477
478
479
480
481
482
483
484
485
486
487
488
489
490
491